A New Core/Shell NiAu/Au Nanoparticle Catalyst with Pt-like Activity for Hydrogen Evolution Reaction

Haifeng Lv[†,‡,∥], Zheng Xi[†,∥], Zhengzheng Chen[§], Shaojun Guo[†], Yongsheng Yu[#], Wenlei Zhu[†], Qing Li[†], Xu Zhang[§], Mu Pan[‡], Gang Lu*[,§], Shichun Mu*[,‡], Shouheng Sun*[,†],

[†]Department of Chemistry, Brown University, Providence, Rhode Island 02912, United States
[‡]State Key Laboratory of Advanced Technology for Materials Synthesis and Processing, Wuhan University of Technology, Wuhan, 430070, China
[§]Department of Physics and Astronomy, California State University Northridge, Northridge, California 91330, United States
[#]School of Chemical Engineering and Technology, Harbin Institute of Technology, Harbin, Heilongjiang 150001, China

[∥]These authors contributed equally.
*To whom correspondence should be addressed.
Email: ganglu@csun.edu; msc@whut.edu.cn; ssun@brown.edu

Experimental Section

Materials: Oleylamine (OAm,>70%), butylamine (99%), oleic acid (OA, technical grade, 90%), 1,2,3,4-tetrahydronaphthalene (tetralin), borane t-butylamine, borane tributylamine, Ni(acac)$_2$ (acac = acetylacetonate) (99.99%), Fe(acac)$_2$ (99.99%), Co(acac)$_2$ (99.99%), hexane (98.5%), ethanol (100%) and Nafion (5% in a mixture of lower aliphatic alcohols and water) were purchased from Sigma Aldrich. Hydrogen tetrachloroaurate (III) hydrate (HAuCl$_4$•3H$_2$O) was purchased from Strem Chemicals. The C-Pt catalyst (20% mass loading, Pt particle size 2.5-3.5 nm in diameter) was obtained from Fuel Cell Store. The deionized water was obtained from a Millipore Autopure system. All the reagents were of analytical grade and used without further purification.

Synthesis of 10 nm Ni$_{43}$Au$_{57}$ NPs. Under a gentle flow of nitrogen (N$_2$) and magnetic stirring, 0.2 mmol of HAuCl$_4$ •3H$_2$O, 9 mL of OAm, and 0.32 mL of OA were mixed, sonicated and heated at 60 °C for 20 min. Once a clear solution was formed, the Ni(acac)$_2$ solution in OAm (0.25 mmol of Ni(acac)$_2$ dissolved in 3 mL of OAm) was added and the solution was further heated to 220 °C at a heating rate of 4-5 °C/min. The solution was kept at this temperature for another 30 min before it was cooled down to room temperature. The product was separated from the reaction solution by adding 40 mL of isopropanol and centrifuging at 8500 rpm for 8 min. The product was re-dispersed in 30 mL of

hexane and precipitated out by adding 30 mL ethanol. The product was further re-dispersed in 20 mL hexane and precipitated out by adding 40 mL ethanol. After centrifugation and solvent removal, the product was re-dispersed in hexane for further use.

In the same reaction condition, reacting 0.2 mmol of $HAuCl_4 \cdot 3H_2O$ with 0.32 and 1.3 mmol of $Ni(acac)_2$ yielded $Ni_{59}Au_{41}$ and $Ni_{34}Au_{66}$ NPs respectively, while with 0.25 mmol of $Fe(acac)_2$ gave $Fe_{47}Au_{53}$ NPs, and with 0.22 mmol of $Co(acac)_2$ produced $Co_{44}Au_{56}$ NPs.

10 nm Au NPs. These NPs were synthesized as described[1].

4 nm Ni NPs. These NPs were synthesized as described[2]. Using this method, we could only obtain 4 nm Ni NPs.

Characterization. NP compositions were measured by inductively coupled plasma-atomic emission spectroscopy (ICP-AES) (JY2000 Ultrace ICP Atomic Emission Spectrometer equipped with a JY AS 421 autosampler and 2400g/mm holographic grating). X-ray diffraction (XRD) patterns of the NP samples were collected on a Bruker AXS D8-Advanced diffractometer with Cu Kα radiation ($\lambda = 1.5418$ Å). Transmission electron microscopy (TEM) images were acquired from a Philips CM 20 (200 kV). High-resolution TEM (HRTEM) images and atomically resolved scanning TEM images along with energy dispersive spectroscopy (EDS) were obtained on a Fei Tecnai Osiris (200 kV).

Catalyst preparation. The as-synthesized NPs were first deposited on Ketjen carbon (C) support by sonicating the C and NP hexane dispersion (C/NP mass ratio = 2:1). The supported NPs, C-NPs, were suspended in butylamine for 3 days at room temperature under constant magnetic stirring to remove the surfactant before they were collected via centrifugation (8500 rpm, 8 min) and washed with ethanol twice and deionized water once[3,4]. The C-NPs were then suspended in deionized water/ isopropanol/Nafion (5%) (v/v/v = 4/1/0.05) to form a 2 mg mL^{-1} ink, 20 μL of which was deposited on the surface of glassy carbon electrode (5 mm diameter) and dried at ambient condition[5] .

Electrochemical studies were conducted using a Autolab 302N potentiostat (Eco Chemie B.V, Holland) with a three-electrode cell setup with a gold wire serving as the counter electrode and Ag/AgCl (4 M KCl) as the reference electrode. The potentials measured were then calibrated against the reversible hydrogen electrode (RHE). Before data collection, all working electrodes were pre-treated by a steady-state potential sweeping from 0 to 1.2 V at 50 mV/s for 100 cycles in N_2-saturated 0.5 M H_2SO_4 solution to remove surface contamination. Once the current-potential curve was stable, the cyclic voltammogram (CV) at 50 mV/s was recorded. Linear sweep voltammetry with scan rate of 2 mV s^{-1} was used to measure HER, the scan rate of the cycling test is 100 mV s^{-1}

Reference electrode calibration. Ag/AgCl (4 M KCl) was used as the reference electrode in all measurements and all potentials were calibrated *vs* revisable hydrogen electrode (RHE). The calibration was performed in 0.5 M H_2SO_4 saturated with Purity Plus Specialty hydrogen (99.99999%) with a Pt wire as the working electrode. The potential was scanned from -0.30 to -0.15 V *vs* Ag/AgCl at a scan rate of 1 mV s^{-1} and the corresponding cyclic voltammogram (CV) was recorded as below. The average of the two potentials at which the current crossed zero was taken as the thermodynamic potential for the hydrogen electrode reactions[6]. The RHE potential was calculated as

E (RHE) = E (*vs* Ag/AgCl) + 0.223 V.
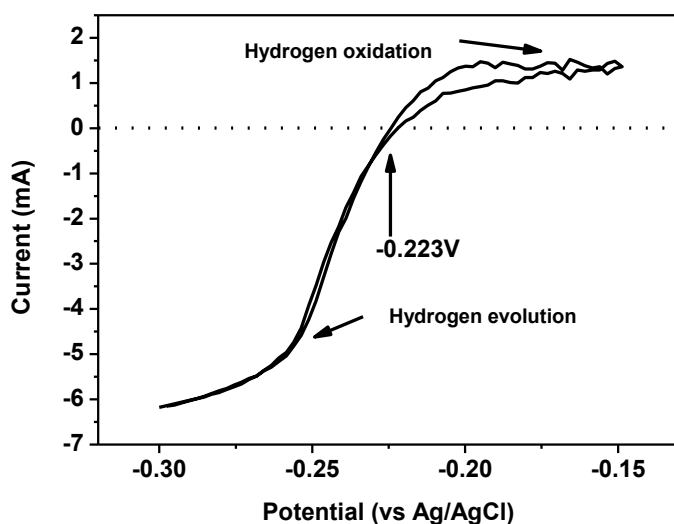
Calculations. All first-principles calculations were performed with the Vienna ab initio simulation package (VASP)[7-9]. Generalized gradient approximation with revised Perdew-Burke-Ernzerhof (RPBE) functional[10] was used in conjunction with projector augmented wave method[11]. A 4-layer 5×3 slab (120 atoms) was employed to represent the Au (111) surface with the lattice constant a = 4.167 Å (See **Figure S5A**). The thickness of the vacuum layer is 15 Å. We have also examined a high-index Au (854) surface to model the presence of (111) surface steps and kinks as shown in **Figure S5B.** Six (111) layers with 64 atoms were included in the computational slab. The energy cutoff was 400 eV and the integration in the first Brillouin zone was performed by 4×4×1 Monkhorst-Pack[12] k-point mesh for the Au (111) surface and 6×4×1 k-point mesh for the Au (854) surface, respectively. A Fermi-Dirac smearing width of 0.02 eV was employed. An isolated Ni site was generated by replacing a Au atom at the (111) surface by a Ni atom. To generate an under-coordinated Au site on the (111) surface, we selected an Au atom at the center of the slab and removed its neighbor atoms one by one, as shown in

Figure 4A. On the Au (854) surface, we have labeled Au sites with n=9 (flat terraces), 7 (steps) and 6 or 8 (kinks). A hydrogen atom was placed at the selected Au or Ni site on the Au (111) and Au (854) surfaces. For Au (111) surface, the bottom two atomic layers were fixed to their equilibrium bulk structure during the atomic relaxation. For the Au (854) surface, only the three top (111) terraces were allowed to relax. The geometric relaxation continued until the Hellmann-Feynman force on each un-constrained atom was smaller than 0.02 eV/Å. As shown in **Table S1**, the results of E_{H*} at Au sites with the same n on Au (111) and Au (854) surfaces are very close to each other. We thus only present E_{H*} on Au (111) surface for clarity.

The free energy diagram for HER was obtained by calculating the change of free energy with a hydrogen atom adsorbed on the Au surfaces based on the computational hydrogen electrode (CHE) [13,14]. The reaction

$$H^+ + e^- \leftrightarrow H_2(g)/2$$
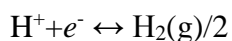
is defined to be in equilibrium at a zero bias voltage, any pH values and temperature with pressure of gaseous H_2 at 1 atm. Therefore, in the context of the CHE model, we have the following relation in chemical potential μ of various species at the zero bias voltage

$$\mu(H^+) + \mu(e^-) = \mu(H_2(g))/2.$$

With this relation, we can bypass the difficulty of calculating the chemical potentials of proton and electron by calculating the chemical potential of gaseous H_2 only. Neglecting PV term in the ambient condition, the free energy can be expressed as

$$G = E + E_{ZPE} - TS,$$

Where E is electronic energy obtained from the first-principles calculations, E_{ZPE} is zero-point energy, and S is entropy. We can then determine hydrogen adsorption free energy, G_{H*}, as follows

$$G_{H*} = G(surf+H) - G(surf) - \mu(H_2(g))/2 = E(surf+H) - E(surf) - E(H_2(g))/2 + \Delta E_{ZPE} - T\Delta S,$$

Where ΔE_{ZPE} is the difference in the zero point energy between the adsorbed H atom and the gaseous phase H_2; ΔS is the difference in entropy. In the present work, we only considered the vibrational entropy, which was calculated based on the phonon frequencies. ΔE_{ZPE} and $T\Delta S$ can be calculated by the data listed in Table S2 at $T = 300$ K. Finally, we have the following equation:

$$G_{H*} = E(surf+H) - E(surf) - E(H_2(g))/2 + 0.24.$$

ΔE_{ZPE} and $T\Delta S$ of the gaseous phase H_2 were taken from Ref.13. This equation is used throughout the

calculations of G_{H*}.

We also calculated local density of states (LDOS) projected onto three representative Au sites: the Au atom on the flat (111) surface ($n = 9$), the Au atom attaching to a step ($n = 5$) and an isolated Au adatom ($n = 3$) as shown in **Figure 4B.** With the decrease of n, the d-band center, E_d, shifts towards the Fermi energy E_F. (E_d = -3.25 eV when $n = 9$, E_d = -3.00 eV when $n = 5$, and E_d = -2.83 eV with $n = 3$). According to the well-known d-band model, the d-band center correlates to the adsorption energy.[15,16] The closer the d-band center to the Fermi energy, the stronger the binding energy, and the lower the G_{H*} value.
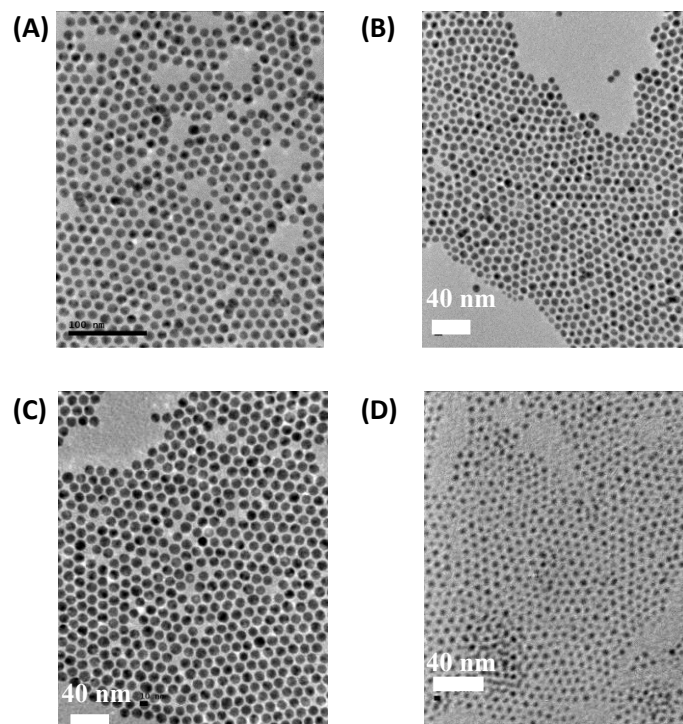
Figure S1 TEM images of the 10 nm $Fe_{47}Au_{53}$ (**A**), $Co_{44}Au_{56}$ (**B**), Au (**C**), and 4 nm Ni NPs (**D**).

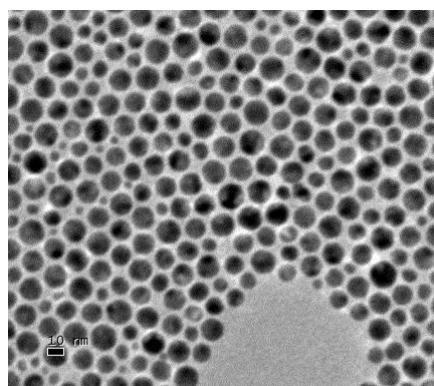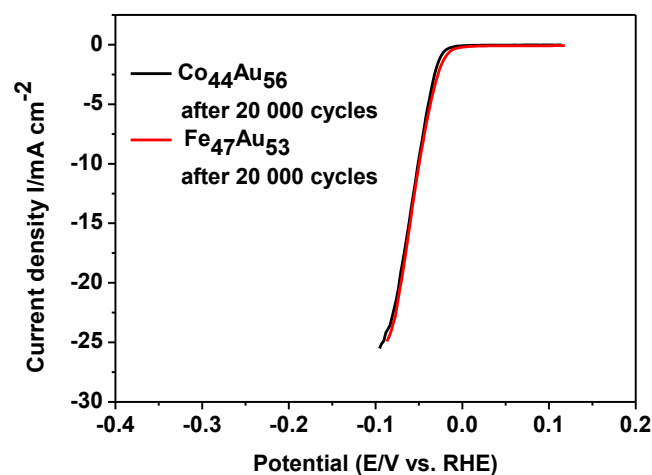**Figure S2.** A typical TEM image of Au NPs made from the reaction when no $Ni(acac)_2$ was added.

Figure S3. HER polarization curves of C-$Co_{44}Au_{56}$ and C-$Fe_{47}Au_{53}$ NPs after 20 000 cycling tests.
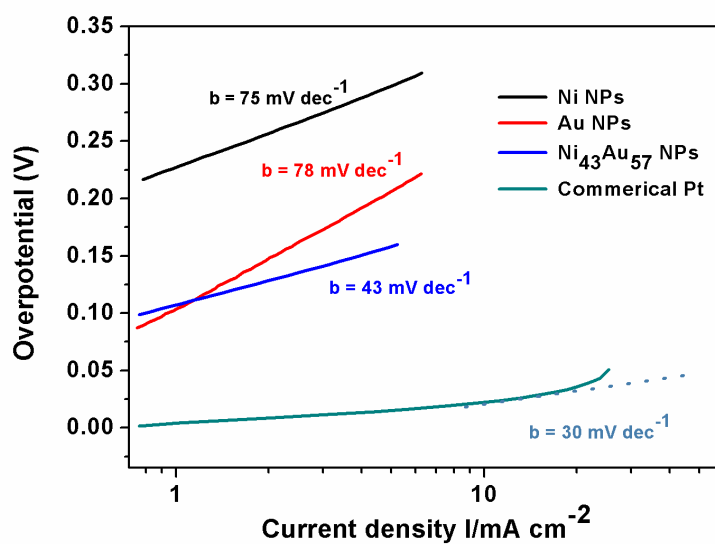

Figure S4. Tafel plots recorded on the corresponding catalysts in 0.5 M H_2SO_4 solution (with a scan rate of 2 mV s^{-1}).
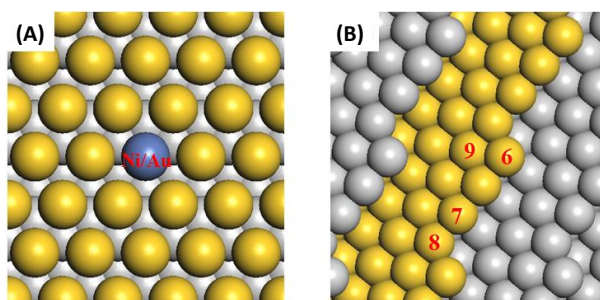
Figure S5. Atomic structures of (**A**) Au (111) and (**B**) Au(854) surfaces. The top layer for hydrogen adsorption is highlighted in gold. The blue sphere in (**A**) represents the chosen Au site and the Ni site. The numbers in (**B**) represent Au sites with different coordination number n.

Table S1 Adsorption energy of the hydrogen atom E_{H*} at Au sites with different n on both Au (111) and Au (854) surfaces.

	n	9	8	7	6
E_{H*} (eV)	Au(111)	0.55	0.47	0.41	0.35
	Au(854)	0.55	0.50	0.44	0.35

Table S2 The zero-point energy and vibrational entropy at $T = 300$ K to the hydrogen atom adsorption on Au surfaces and a gaseous H_2 molecule.

	TS	E_{ZPE}
H_2[13]	0.41	0.27
H*	0.02	0.19

References

1. Zhu, W. L.; Michalsky, R.; Metin, Ö.; Lv, H. F.; Guo, S. J.; Wright, C. J.; Sun, X. L.; Peterson, A. A.; Sun, S. H. *J. Am. Chem. Soc.* **2013,** 135, 16833-16836.

2. Metin, Ö.; Mazumder, V.; Özkar, S.; Sun, S. H. *J. Am. Chem. Soc.* **2010,** 132, 1468-1469.

3. Guo, S. J.; Zhang, S.; Wu, L. H.; Sun, S. H. *Angew. Chem.* **2012**, 124, 11940-11943.

4. Wu, J.; Zhang, J.; Peng, Z., Yang, S.; Wagner, F. T.; Yang, H.; *J. Am. Chem. Soc.* **2010,** 132, 4984-4985.

5. Lv, H. F.; Cheng, N. C.; Peng, T. Pan, M.; Mu, S. C. *J. Mater. Chem.*, **2012**, 22, 1135-1141.

6. Liang, Y. Y. Li, Y. G.; Wang, H. L.; Zhou, J. G.; Wang, J.; Regier, T.; Dai, H. J. *Nature Mater.* **2011,** 10**,** 780-786.

7. Kresse, G.; Hafner, J. *Phys. Rev. B.* **1993,** 47, 558-561(R).

8. Kresse, G.; Hafner, J. *Phys. Rev. B*, **1994,** 49, 14251-14269.

9. Kresse, G.; Hafner, J. *Comput. Mater. Sci.*, **1996,** 6, 15-50.

10. Hammer, B.; Hansen, L. B.; Nørskov, J. K. *Phys. Rev. B.* **1999,** 59, 7413-7421.

11. Kresse, G.; Joubert, D. *Phys. Rev. B.* **1999,** 59, 1758-1775.

12. Monkhorst, H. J.; Pack, J. D. *Phys. Rev. B.* **1976,** 13, 5188-5192.

13. Nørskov, J. K. Rossmeisl, J.; Logadottir, A.; Lindqvist, L. *J. Phys. Chem. B*. **2004,** 108, 17886-17892.

14. Peterson, A. A.; Abild-Pedersen, F.; Studt, F.; Rossmeisl, J.; Nørskov, J. K. *Energy Environ. Sci.* **2010,** 3, 1311-1315.

15. Mavrikakis, M.; Hammer, B.; Nørskov, J. K. *Phys. Rev. Lett.* **1998**, 81, 2819-2822.

16. Hammer, B; Nørskov, J. K. *Nature* **1995**, 376, 238-240.